Polymer xxx (2016) xxx-xxx

Contents lists available at ScienceDirect

Polymer

journal homepage: www.elsevier.com

Functional supramolecular tetrathiafulvalene-based films with mixed valences states

Marta Riba-Moliner [a], Andrés Gómez-Rodríguez [a], David B. Amabilino [b], Josep Puigmartí-Luis [c], Arántzazu González-Campo [a, *]

[a] Institut de Ciència de Materials de Barcelona (ICMAB-CSIC), Campus Universitari de Bellaterra, 08193, Cerdanyola del Vallès, Spain
[b] School of Chemistry, University of Nottingham, University Park, NG7 2RD, Nottingham, UK
[c] Empa, Swiss Federal Laboratories for Materials Science and Technology, Lerchenfeldstrasse 5, 9014, St. Gallen, Switzerland

ARTICLE INFO

Article history:
Received 2 May 2016
Received in revised form 8 September 2016
Accepted 13 September 2016
Available online xxx

Keywords:
Polymer
Tetrathiafulvalene (TTF)
Thin film
Poly(4-vinyl pyridine) (P4VP)
Mixed valence state
Hybrid polymer
Electrostatic Force Microscopy (EFM)
Charge transport
Hydrogen bonding

ABSTRACT

Tetrathiafulvalene molecules substituted with a carboxylic acid group (TTFCOOH) were bound as redox-active moieties into a poly(4-vinyl pyridine) (P4VP) skeleton through non-covalent interactions (hydrogen bonds). The aspect of the resulting P4VP-TTFCOOH films showed a uniform and smooth morphology. Moreover, the redox function of TTFCOOH in P4VP-TTFCOOH was demonstrated using tetrachloroauric acid, iron(III) perchlorate and iodine vapors as doping agents. The oxidized states of TTFCOOH as well as the mixed valance state $TTFCOOH^{0}$-$TTFCOOH^{+\bullet}$ were generated in a controlled manner in solid state, resulting in an organic film capable of charge transport. The charge transport along the organic donor molecules hydrogen bonded to the polymer matrix was demonstrated employing Electrostatic Force Microscopy (EFM).

1. Introduction

The non-covalent functionalization of polymers via supramolecular chemistry is a potentially efficient route to introduce a particular property with which a new functional molecular material can be originated. Functional polymers can be described as one class of molecular materials where function can be achieved through the incorporation of active side-groups and provide particular properties to the final construct [1]. Interestingly, the incorporation of conjugated structures in polymeric constructs has been already exploited to synthesize new semiconducting materials that have found application in many fields including photovoltaics [2,3]. Although important advances have been made in this field, the incorporation of π-electron functional units to polymeric backbones with well-controlled arrangement between the donor and acceptor parts is still an area of huge interest for materials science. In this regard, the incorporation of hydrogen bond donating or accepting site groups has allowed the formation of new polymeric supramolecular assemblies through hydrogen-bonding interactions. The principles of this kind of approach have been laid for some systems, notably containing pyridine as the hydrogen bond acceptor [4–6].

Poly(4-vinyl pyridine) (P4VP) has become a widely used polymer to prepare new functional composite materials. Sugiyama and Kamogawa demonstrated that the basic character of the nitrogen atom present in the pyridyl unit can be advantageously used for the formation of charge-transfer complexes with quinone moieties [7,8]. The nitrogen atom in P4VP provides an anchoring point where various compounds can be incorporated with the objective to add functionality to the final polymeric construct. Indeed, there are many studies showing the functionalization of P4VP through non-covalent hydrogen bond interactions [4,8,9]. This strategy has become important to prepare organic semiconductor-based films with control over the nanoscopic assembly of organic molecules and to obtain charge mobility within films. Slough and co-workers found a variation in the conductivity of donor polymers with the incorporation oligothiophene to P4VP and obtain uniform films that can be used as *p*-type semiconductors using solution processing methods [10]. Very recently, a complex between P4VP and a rylenebisimide derivative −used as an electron accepting component− also permitted the formation of a material with charge transport properties similar to those of the acceptor alone, providing best evidence of the promise of this approach for the preparation of n-type organic semiconductors [11].

In this paper, the combination of P4VP with an electron donating unit based on a tetrathiafulvalene (TTF) derivative is presented. Tetrathiafulvalenes (TTFs) are excellent π-electron donor units that are widely studied in molecular electronic applications due to their *p*-type character and stable doped states [12,13]. As electron-donor species, TTFs can be oxidized reversibly under their exposure to an appropriate oxidant and/or reducing agent. Three oxidization states are present in TTFs, the neutral TTF (TTF^{0}), which exists under am-

* Corresponding author.
Email address: agonzalez@icmab.es (A. González-Campo)

http://dx.doi.org/10.1016/j.polymer.2016.09.039
0032-3861/

bient conditions, the cation-radical ($TTF^{+\bullet}$) and the dication (TTF^{2+}) state that are prepared by chemical or electrochemical oxidation of the neutral compounds. The three states can be accessed and controlled sequentially through one electron processes. Furthermore, TTF derivatives can form highly ordered mono- or bi-dimensional stacks through π–π interactions between the planar core as well as through side-by-side sulfur-sulfur interactions between the neighboring TTF units [14,15]. The ability to control the self-assembly of TTF derivatives have attracted a great deal of attention in the materials science field because TTF-based supramolecular assemblies can lead to functional conductive materials. Cai and coworkers took advantage of the self-assembly through π-π interactions of TTFs to build 2-D covalent organic frameworks (COFs) with conducting properties [16]. For instance, Yokota et al., embedded thiol-terminated TTFs into a *n*-alkanethiol matrix and observed how strong was the influence of the intermolecular electronic coupling of them by applying different values of voltages [17]. The capacity of TTF derivatives to generate mixed-valence states by UV-irradiation in polymer matrices of PMMA containing a photo-induced acid generator has also been studied by Tanaka et al., showing the regulation of TTF electronic states by photo-reaction in TTF-based polymeric films [18]. Recently, the same authors have also synthesized TTF-tethered polymeric films and demonstrated the conductivity of this material thanks to the formation of a TTF mixed-valence state generated after the oxidation of the TTF units [19]. The continuous research and the desire to improve the efficiency and performance of organic field-effect transistors (OFETs), has also made TTFs and its derivatives key and interesting compounds for the development of new polymeric organic charge-carrier systems [20]. For example, Chujo et al. introduced composite TTF-based polymer thin films employing conventional polymers such as poly(methyl methacrylate) (PMMA) and poly(styrene) (PS) as the polymer matrix. Furthermore, the authors also demonstrated the charge transport properties of these TTF-based polymer composites comparing them with a common conductive polymer blend used as a reference material, i.e. poly(3,4-ethylenedioxythiophene)-poly(styrene sulfonate) (PEDOT-PSS) [21].

In the present work, we report the preparation of supramolecular polymeric films generated by the incorporation of a TTF derivative (TTFCOOH) to P4VP (Scheme 1). The TTFCOOH has been designed with a carboxylic acid group (-COOH), to allow hydrogen bond formation with the pyridyl groups of P4VP, and with two long alkyl chains to ease solubility. As result of the interaction between TTF-COOH and P4VP, a new composite material is formed with unique synergistic functionalities (vide infra) (P4VP-TTFCOOH, Scheme 1), The properties of the final construct were studied by UV-vis-NIR absorption spectroscopy, FT-IR-NIR spectroscopy, Transmission Electron Microscopy (TEM), Scanning Electron Microscopy (SEM), Energy Dispersive X-rays (EDX), Electron Paramagnetic Resonance (EPR), and Scanning Probe Microscopy (SPM) techniques such as Electrostatic Force Microscopy (EFM). SPM techniques can provide information about the phase segregation of the constituent compounds present in the sample, the surface potential of the composite polymeric film, and further, can be employed to study charge transport in the films generated [22].

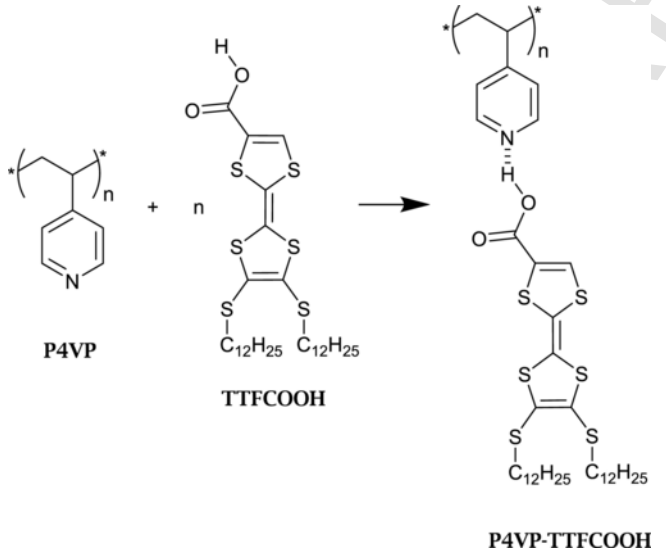

Scheme 1. Formation of P4VP-TTFCOOH through the hydrogen bond formation between P4VP and TTFCOOH.

2. Materials and methods

2.1. Materials

4-vinyl pyridine (containing 100 ppm hydroquinone as inhibitor), α-methylstyrene 99% (containing 15 ppm *p-tert*-butylcatechol as inhibitor), the initiator *sec*-butyllithium (1.4 M in cyclohexane), $HAuCl_4{\cdot}3H_2O$ (gold(III) chloride trihydrate ≥99.9% trace metal basis), $Fe(ClO_4)_3$ (iron(III) perchlorate hydrate crystalline), I_2 (≥99.99% trace metals basis) and methanol (anhydrous, 99.8%) were purchased from Sigma-Aldrich. THF (HPLC degree) was purchased from Teknokroma. TTFCOOH was synthesized in a previous work following the literature procedure [23].

2.2. Synthesis of P4VP

P4VP was synthetized using living anionic polymerization based on the procedure that Varshney et al. [23] described. 4-vinyl pyridine was distilled and tetrahydrofuran (THF) was dried with sodium/benzophenone before used. α-methylstyrene was previously dried by distillation over calcium hydride. A solution of 1.5 mmol of α-methylstyrene in THF was prepared. Then, *sec*-butyllithium was added dropwise to the mixture using a stainless steel syringe until the color of the solution persisted. The color of the solution was given by the formation of the α-methylstyryllithium (α-MS–Li^+) as a product of the reaction of α-methystyrene and *sec*-butyllithium. Then, the reaction was cooled down to −78 °C and 32 mmol of 4-vinyl pyridine was added slowly, observing a sudden change of the color of the initiator (from red to light yellow). The polymerization was ended by adding methanol and the precipitation of the polymer $(C_7H_7N)_n$ occurred. Afterwards, the polymer was recovered by precipitation in hexane and it was thoroughly dried under vacuum. ^1H NMR $(C_7H_7N)_n$ ($CDCl_3$, 300 MHz), δ_H (ppm): 1.27–1.79 (br, 3H), 6.22–6.56 (m, 2H), 8.15–8.58 (m, 2H). M_w (GPC) $(C_7H_7N)_n$: 358 g/mol.

2.3. Self-assembly of P4VP-TTFCOOH and film formation

A solution of P4VP and TTFCOOH (10 mM, 1:1 M ratio) in chloroform was prepared and vigorously stirred. Films were obtained by spin-coating 170 μl of the as-prepared solution on a surface and allowing the evaporation of the solvent. The conditions used for film sample formation were: 4000 or 5500 rpm of acceleration and 30 s of rotation. In the case of drop casted films, samples were prepared by

depositing a droplet of P4VP-TTFCOOH solution on the surface and letting it to evaporate at room temperature.

2.4. Oxidation in solution

A solution of P4VP and TTFCOOH (10 mM, 1:1 M ratio) in chloroform was prepared. An aliquot of 10 μl was diluted in 3 ml of acetonitrile and transferred into a 10.00 mm path quartz cuvette. Meanwhile, solutions of $HAuCl_4$ 0.015 M and $Fe(ClO_4)_3$ 0.0150 M in chloroform were prepared separately. To follow the oxidation of P4VP-TTFCOOH in solution, addition of the oxidizing solutions to the UV-visible quartz cuvette was progressively conducted in both cases and in separate experiments.

2.5. Film oxidation

In order to study the oxidation process of the as-prepared films, doping cycles by immersing the films on quartz support in an aqueous solution (Milli-Q grade) of the oxidizing agent under study was conducted. In all cases, the immersion time was established to be 10 min. Then, the film was dried with N_2 flow, washed by immersion in H_2O (Milli-Q grade) for 1 min, and dried with a flow of nitrogen gas. The molar ratio TTFCOOH:oxidizing agent was 25:1 for $HAuCl_4$, as well was for $Fe(ClO_4)_3$. In the case of I_2 vapors, the films were doped by exposing them to I_2 vapors for 3 s in a sealed container, without further washing (Fig. S1).

2.6. Instrumentation

A double beam UV-vis-NIR spectrophotometer Varian Cary 5000 with operational range of 190–3300 nm was used to conduct the UV-vis spectroscopic measurements. FTIR spectra were acquired in a Spectrometer Perkin-Elmer Spectrum One with an energy range of 450–4000 cm^{-1}. For SEM and EDX analyzes samples were measured at high and low vacuum conditions where the electron beam acceleration voltage was set between 10 kV and 20 kV. SEM QUANTA FEI 200 FEG-ESEM microscope equipped with a field emission gun (FEG) for optimal spatial resolution was used. The instrument could be used in high vacuum mode (HV), low-vacuum mode (LV) (water vapour injection), and environmental SEM mode (ESEM), depending on the stability of samples. The microscope was equipped with an Energy Dispersive X-ray (EDX) system for chemical analysis. All EFM measurements were performed with a 5500LS SPM system from Agilent Technologies with Nano World Pointprobe silicon SPM sensor tips, provided with a force constant of 2.8 N/m, a coating tip side of Pt/Ir, and a coating detector side of Pt/Ir. The measurements were conducted under controlled atmospheric conditions by flowing compressed air and N_2, to reach 3.5–5.0% of relative humidity. Set-point values of 2.47 V and 1.9 V were fixed to image areas of 2 × 2 μm and 5 × 5 μm respectively. Previously, set-point voltage values were calibrated and referenced to the height between the sample surface and the tip (1V–30 nm). A 120 KV JEOL 1210 TEM microscope with a high angular range (Tilt X = ± 60°, Tilt Y = ± 30°) for exploring large volumes of the reciprocal lattice by electron diffraction with a resolution below 3.2 Å was used for TEM imaging. A Bruker ELEXYS E500 × band EPR spectrometer equipped with a variable temperature unit, a field frequency (F/F) lock accessory, and built in NMR Gaussmeter was used to measure EPR spectra. The equipment used to determine the film thickness was a GES5E Optical Platform ellipsometer from Sopra which allowed various measurement modes from standard ellipsometry to generalized ellipsometry going through photometric measurements (in Transmission and Reflection), scatterometry, and luminescence measurements. The standard spectral range of it was 230–900 nm and the measurement angles ranged from 10° to 90°.

3. Results and discussion

3.1. Self-assembly of P4VP-TTFCOOH

The complexation between P4VP and TTFCOOH is generated through the hydrogen bond formation between the acid group of TTFCOOH with the nitrogen atom of the pyridine rings present in the polymeric matrix (Scheme 1) [24–26]. In order to ensure the complete supramolecular assembly of TTFCOOH, solubility studies were performed in where chloroform was first identified as the most suitable solvent for the experiments because is an organic and non-polar solvent that dissolved both P4VP and TTFCOOH. In this way, chloroform-based solutions and thin films of the polymer with TTFCOOH were prepared and their homogeneity and thickness were studied. To synthesize thin films of P4VP-TTFCOOH, we first employed the drop-casting method, however spin-coating was the strategy finally followed in our investigations because a higher homogeneity and reproducibility of the films generated was obtained.

FTIR spectroscopy was used to trace the formation of P4VP-TTFCOOH following the shift of characteristic bands of the free pyridine ring located at 1596 cm^{-1}, 1413 cm^{-1} and 993 cm^{-1} upon the non-covalent hydrogen bond interaction with TTFCOOH, (Fig. 1) [11,27,28]. The FT-IR spectrum of P4VP-TTFCOOH films revealed a decrease of intensity and a shift of the bands located at 993 cm^{-1} and 1596 cm^{-1} to 1030 cm^{-1} and 1608 cm^{-1}, respectively, confirming the hydrogen bond between P4VP and TTFCOOH. It was not possible to trace the band at 1415 cm^{-1} due to the presence of a band around 1422 cm^{-1} for pure TTFCOOH in the same region. On the other hand, the disappearance of the ν(C═O) stretching vibration transmission band at 1663 cm^{-1} and the appearance of a new band at 1694 cm^{-1} were associated to the coordination of TTFCOOH moieties to the nitrogen atoms of the pyridine rings present in the polymer matrix. This change is typically related with systems having hydrogen bonds, providing further evidence that the assembly between

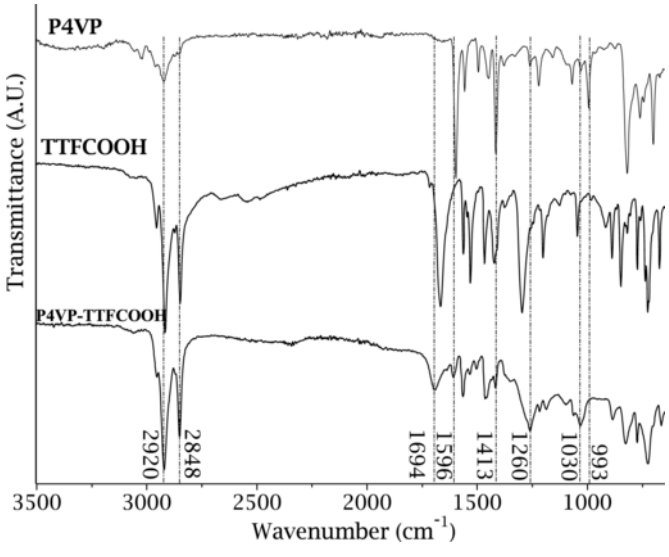

Fig. 1. FT-IR spectra of P4VP, TTFCOOH and P4VP-TTFCOOH films.

the carboxylic acid group of TTFCOOH and the nitrogen atom of the pyridyl unit present in P4VP took place [21,27–29]. The bands at 2920 cm^{-1} and 2848 cm^{-1}, which appeared for TTFCOOH and P4VP, were associated to the ν_{as}(C—H) and ν_{sym}(C—H) of the alkyl chains of the hydrogen bonded composite film.

The formation of P4VP-TTFCOOH was also studied comparing the UV-visible absorption spectra obtained from drop-casted solutions of pure TTFCOOH and a mixture of poly(styrene) and TTFCOOH (PS + TTFCOOH) on quartz surfaces. The latest was studied as a control sample; in this case the non-covalent assembly between the carboxylic acid group of TTFCOOH molecules and the polymer matrix is avoided. As shown in Fig. 2, the broad peak at 510 nm for pure TTFCOOH and PS + TTFCOOH was associated to free and non-coordinated TTFCOOH moieties. Contrarily, the spectrum of P4VP-TTFCOOH films showed an absorption band at 416 nm. The blue shift observed of this band was attributed to the increase of electron density of the TTFCOOH due to the hydrogen bonding interaction with the pyridines groups of the P4VP [30]. Another evidence of the non-covalent assembly of TTFCOOH molecules to the pyridyl units of P4VP was the slight shift of the band located at around 306 nm when compared to pure TTFCOOH and PS + TTFCOOH samples.

The chemical resistance of P4VP-TTFCOOH films was studied at different pH values by UV-visible spectroscopy [31]. After immersing the films in the different solutions and varying the pH value, it could be concluded that the films are stable between $2 \leq pH \leq 10$. However, in strongly basic media, a shift in the peak at 416 nm evidences a chemical change in the film construct. Concretely, at values above 9, a decrease of the band at 416 nm and an initial red-shift was observed, resulting in two isosbestic points at 349 nm and 433 nm, which undoubtedly indicated a modification of the film structure probably due to the deprotonation of the carboxyl group of TTFCOOH (Fig. 3).

3.2. Doping and film oxidation

Previously, our group has demonstrated that materials based on TTF derivatives can be oxidized (doped) easily under certain conditions [32,33]. Solutions of different oxidizing agents such as $HAuCl_4$ and $Fe(ClO_4)_3$ in $CHCl_3$ were added to solutions of P4VP-TTFCOOH to study and elucidate the effects of the oxidation of TTFCOOH in the chemical and physical properties of the hydrogen bonded composite films.

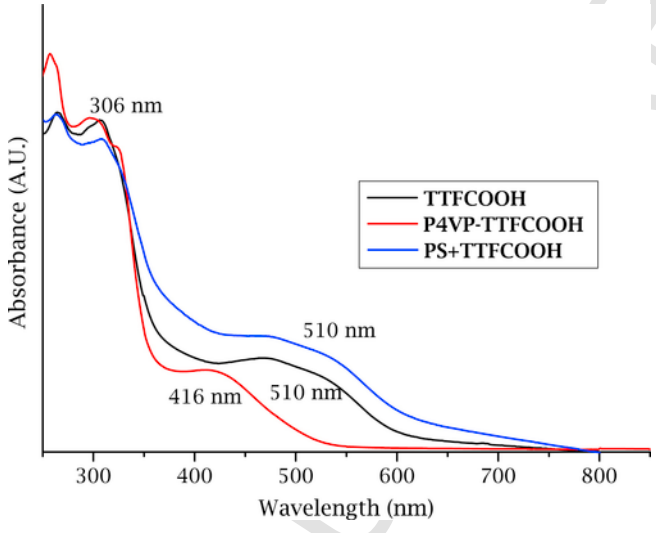

Fig. 2. UV-visible absorption spectra of TTFCOOH, P4VP-TTFCOOH and PS + TTFCOOH drop-casted films. The solvent used to prepare the films was $CHCl_3$ in all the cases.

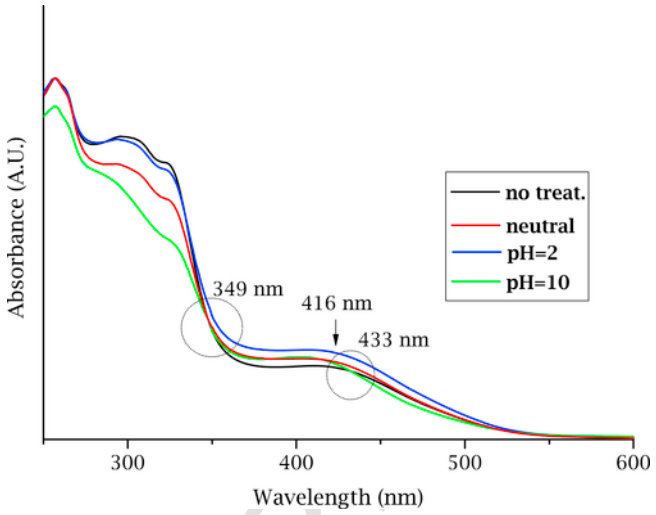

Fig. 3. UV-visible absorption spectra of neat P4VP-TTFCOOH and P4VP-TTFCOOH films after 10 min of immersion in neutral (pH = 7), acid (pH = 2) and basic (pH = 10) solutions. Films were prepared by drop-casting on quartz surfaces. The direction of the arrow indicates increase/decrease or shift of the signal.

The doping processes were first studied in solution and followed by UV-Vis-NIR absorption spectroscopy after the successive addition of oxidants (Fig. 4). During the oxidation process with $HAuCl_4$ a change in the color of P4VP-TTFCOOH solutions was observed, which was an indication that TTFCOOH was oxidized from the neutral state (light orange), to the cation-radical (greenish), and to the dication state (intense blue) (Fig. S1) [33].

UV-Vis-NIR absorption spectra revealed that it is possible to oxidize TTFCOOH molecules to the dicationic state (TTF^{2+}) in the polymer composite supramolecular system with both oxidants, $HAuCl_4$ and $Fe(ClO_4)_3$ (Fig. 4 and Fig. S2). The band at approximately 413–423 nm was attributed to TTF^0, when no doping agent was added. After several additions of $HAuCl_4$, the TTF^0 band progres-

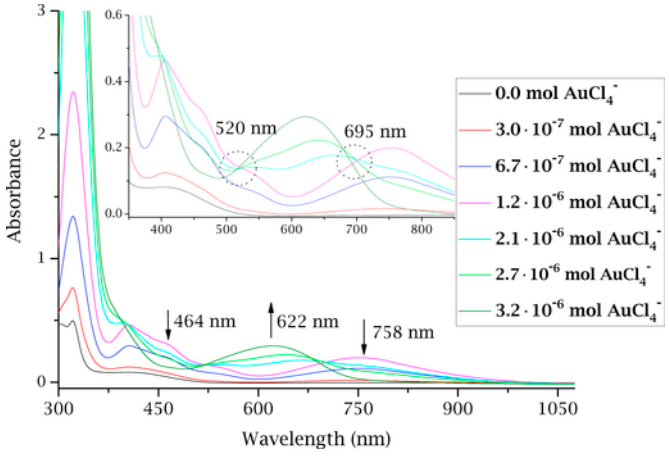

Fig. 4. UV-Vis-NIR absorption spectra showing the evolution of TTFCOOH oxidation in P4VP-TTFCOOH employing $HAuCl_4$ as doping agent. The inset shows the amplified spectra in the range from 350 to 850 nm. The direction of the arrows indicates increase/decrease or shift of the signals.

sively decreased due to the formation of $TTF^{+\bullet}$ species until its total vanishing [32]. Then, a shoulder appeared at 464 nm (437 nm in the case of $Fe(ClO_4)_3$ doping), which indicated the formation of free cation radicals ($TTF^{+\bullet}$) reaching its maximum value at $1.2{\cdot}10^{-6}$ mol of doping agent. Moreover, the appearance of the band at 758 nm was attributed to the formation of π-dimers between cation-radical TTFs (744 nm in the case of $Fe(ClO_4)_3$. This band was subsequently replaced by a band at 622 nm upon further doping, which is characteristic of the formation of TTF^{2+} during the doping process (with $Fe(ClO_4)_3$ as oxidizing agent a slight shoulder at 546 nm also appeared). Moreover, isosbestic points at 520 nm and 695 nm were observed, in the absorption spectra resulting from doping with $HAuCl_4$ (618 nm and 917 nm in the case of $Fe(ClO_4)_3$ doping), which indicated that a clear change in the doped species was produced, *i.e.* $TTF^{+\bullet}$ species were fully oxidized to TTF^{2+} [32].

Once the capacity to oxidize the TTF residues in P4VP-TTFCOOH solutions was confirmed, same studies in solid state were performed to produce doped polymeric films. The oxidation of films was also followed with UV-Vis-NIR absorption spectroscopy using $HAuCl_4$, $Fe(ClO_4)_3$ as well as I_2 vapors as doping and/or oxidizing agents. In this case, the oxidizing agents were dissolved in MilliQ water (except I_2) to ensure the stability of the films. The oxidation process consisted on dipping the films in a solution containing the oxidant in molar ratio of TTFCOOH:oxidizing agent 25:1 for 10 min and then rinsing them in a ultrapure water bath for 10 additional minutes. During the oxidation process and because films were not porous (vide infra), co-existence of all three oxidation states of the TTF units were demonstrated depending on the proximity of TTFCOOH molecules to the oxidant solution or to the substrate. After doping P4VP-TTFCOOH films with $HAuCl_4$ (Fig. 5), the absorption band at 423 nm associated to TTF^0 disappeared while another band at 651 nm appeared after the first doping cycle, which is related with the formation of $TTF^{+\bullet}$ in the polymeric film. Moreover, an absorption shoulder was observed between 816 nm and 1120 nm, which was associated to the formation of a charge transfer band due to the charge mobility between TTF^0 and $TTF^{+\bullet}$ states, as previously reported by us [34].

Therefore, P4VP-TTFCOOH films can induce the assembly of partially oxidized TTF stacks, thanks to the hydrogen bonding formation [35]. In additional doping cycles, the $TTF^{+\bullet}$ band was shifted slightly to a high energy (absorption maximum at 628 nm) and with slightly less intensity, suggesting the formation of TTF^{2+}species, which absorb in that region. An isosbestic point at 587 nm indicated a change from $TTF^{+\bullet}$ states to TTF^{2+}. However, the completely formation of TTF^{2+} could not be reached fully in the film, even after conducting long doping cycles in $HAuCl_4$ solutions. Although a weak charge transfer absorption band could be observed (816 nm and 1120 nm) for the first cycle, a more intense band at 963 nm was observed after the fourth cycle. The appearance of this charge transfer absorption band at lower energy indicated that high charge mobility could be reached between TTF^0-$TTF^{+\bullet}$ units after the first doping cycle. After the fourth cycle (probably because of the presence of intermediate states such as $TTF^{+\bullet}$-TTF^{2+} and other monomers) charge mobility was not favorable [35,36]. The charge transfer band was observed at 892 nm and 948 nm when the film was doped with $Fe(ClO_4)_3$ (Fig. S3) and I_2 vapors (Fig. S4), respectively. Therefore, it was possible to reach the same oxidized state with all doping agents studied [36].

Once the capacity to oxidize the TTF units present in P4VP-TTFCOOH films was proved using different doping agents, the reversibility of the oxidation process for P4VP-TTFCOOH solutions and film samples was also studied. With this aim, we first studied the dedoping of a $HAuCl_4$ doped P4VP-TTFCOOH solution containing $TTFCOOH^{2+}$. Sequential additions of trimethylamine (TEA) in acetonitrile at stoichiometric concentration to the TTF moieties present in P4VP-TTFCOOH solutions were added, in order to reach the completely neutral TTF state. The dedoping process evolution followed by UV-Vis-NIR spectroscopy illustrated the decreasing of the absorption signals at 667 nm and 902 nm associated to the mixed valence state $TTF^{+\bullet}$-TTF^{2+} and the charge transfer band, respectively (Fig. 6). The charge transfer band disappeared practically from cycle nº9 and the mixed valence state still remained, indicating that P4VP-TTFCOOH in solution could be only partially reduced.

Concurrently, this dedoping process was also performed for $HAuCl_4$ doped P4VP-TTFCOOH films by immersing them in a TEA aqueous solution for 10 min. The TEA concentration was stoichiometrically calculated according to the TTF amount present in P4VP-

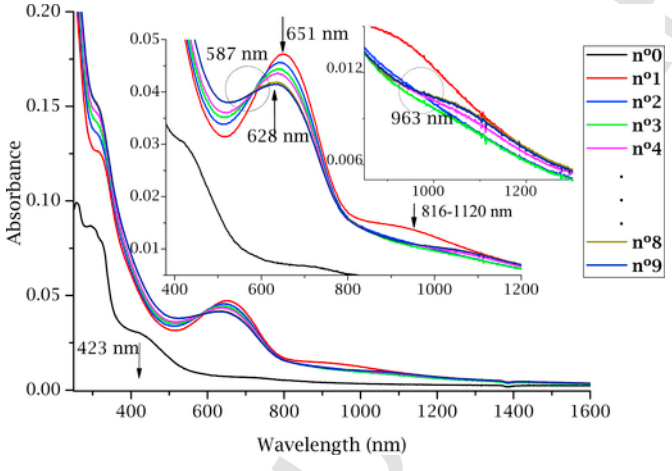

Fig. 5. UV-Vis-NIR absorption spectra of the evolution of oxidation of P4VP-TTFCOOH films on quartz after each doping cycle with $HAuCl_4$ (aq). The insets show the amplified spectra in the range from 400 to 1200 nm and from 850 to 1300 nm, respectively. The numbers of the legend correspond to the number of doping cycles, where 0 is the neat film without treatment. The direction of the arrows indicates increase/decrease or shift of the signals.

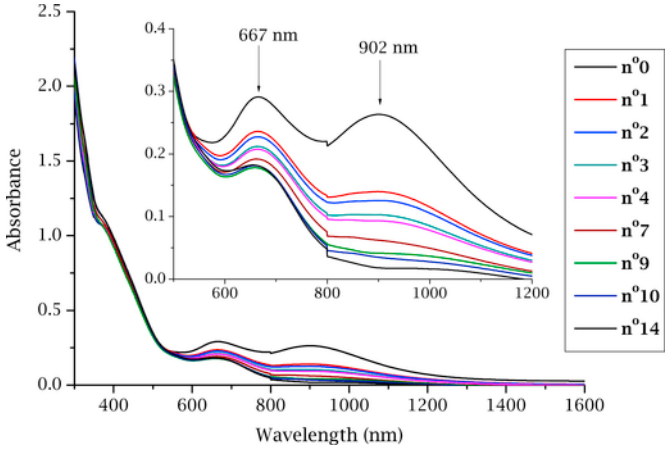

Fig. 6. UV-Vis-NIR absorption spectra showing the evolution of bands during a dedoping process of a P4VP-TTFCOOH solution performed with TEA solution (in the legend, each number after "nº" means the number of immersions). The inset shows the amplified spectra in the range from 500 to 1200 nm. The direction of the arrows indicates increase/decrease or shift of the signals.

TTFCOOH films. After each immersion, the films were washed in an ultrapure water bath for 10 additional minutes to eliminate surplus reagents. The evolution of the dedoping process was followed by UV-Vis-NIR absorption spectroscopy (Fig. 7), corroborating that the doped P4VP-TTFCOOH films could be reduced from $TTFCOOH^{2+}$ to the mixed valence $TTFCOOH^{0}$-$TTFCOOH^{+\bullet}$ state. The spectrum of the doped P4VP-TTFCOOH films showed an absorption peak at 619 nm associated to the $TTFCOOH^{2+}$ state, and was established as starting state of the film in the dedoping process. In subsequent immersions of P4VP-TTFCOOH films in TEA solution, the progressively reduction of $TTFCOOH^{2+}$ units in the polymeric films was observed by the appearance of bands at 415 nm and 440 nm. The appearance of these bands indicated the presence of $TTFCOOH^{+\bullet}$-$TTFCOOH^{2+}$ and $TTFCOOH^{0}$-$TTFCOOH^{+\bullet}$ in the films, respectively. Then, some neutralized $TTFCOOH^{0}$ units were obtained, although the simultaneously absorption signal at 524 nm, suggested that the completely neutral state could not be reached in film samples.

P4VP-TTFCOOH films doped with $HAuCl_4$, $Fe(ClO_4)_3$, and I_2 vapors were also measured by FT-IR-NIR spectroscopy (Fig. 8). A broad charge-transfer band appeared from 5000 cm^{-1} to 2000 cm^{-1}, upon oxidation of the film with any of the doping agents used, which was in concordance with previously reported systems [18]. In addition, we also observed a decrease of the transmittance signal that is assigned to the charge transfer between TTF radicals and neutral TTF moieties. It should be noted that these results are in good agreement with the previous charge transfer bands observed by other UV-visible absorption studies [29,36–41]. Kimura and Cooke et al. observed the appearance of a new band at the region between 1340 cm^{-1} and 1348 cm^{-1}, which was associated with the coupling of a conduction electron with the vibrational mode of the TTF moiety (electronic-molecular vibration coupling) [39,42]. The C═N stretching bands of the pyridine were observed at 1351 cm^{-1} in the undoped film, at 1336 cm^{-1} in the film doped with $HAuCl_4$, at 1388 cm^{-1} in the film doped with $Fe(ClO_4)_3$ and at 1351 cm^{-1} in the film doped with I_2. These little deviations in the υ(C═N) bands are probably related with the orientation of the internal macromolecules when the samples were drop-casted on KBr pellets. According to Mulliken, charge-transfer forces could be related with the orientation and symmetry of the atoms, as well as with the compression applied. This phenomenon

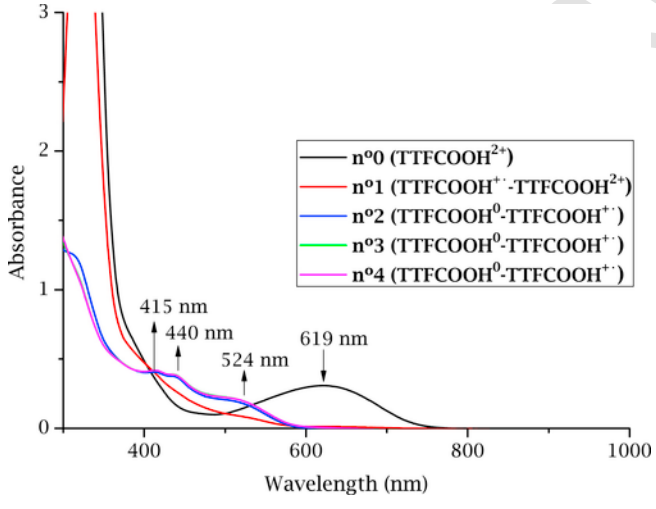

Fig. 7. UV-Vis-NIR absorption spectra of the evolution of TTFCOOH oxidized states in a P4VP-TTFCOOH film after immersion in TEA solution (in the legend, each number after "nº" means the number of immersions). The direction of the arrows indicates increase/decrease or shift of the signals.

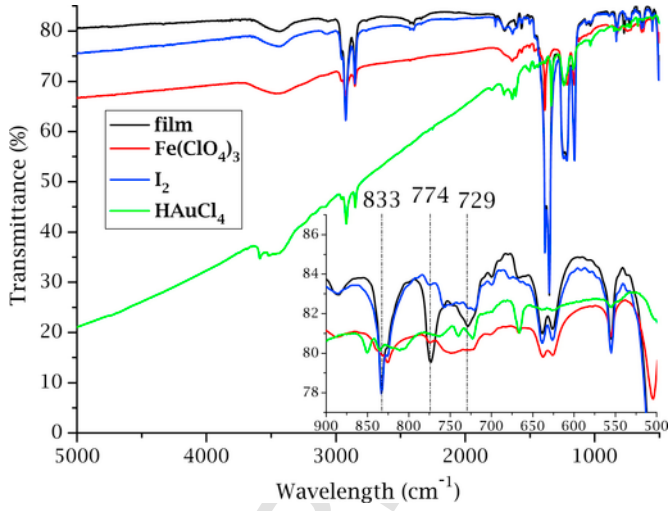

Fig. 8. FT-IR-NIR spectra of P4VP-TTFCOOH films: non-oxidized, and oxidized with $Fe(ClO_4)_3$ (aq), I_2 vapors and $HAuCl_4$ (aq). Samples were prepared by drop-casting solutions on KBr pellets.

can also have a relatively important effect when the samples were doped, affecting the doping grade reached and producing non-desired light scatter effects. Moreover, this could explain the deviations observed in FTIR spectra that had slight differences non-related with molecular bond vibrations [43].

In the fingerprint region of the FT-IR spectra, the absorption band at 833 cm^{-1} disappeared while the bands at 774 cm^{-1} and 729 cm^{-1} slightly decreased and shifted to 724 cm^{-1} after the doping process of the film using $Fe(ClO_4)_3$ and $HAuCl_4$. According to Bozio et al., this change could be attributed to changes in the polarization and symmetry of the TTF moieties [29]. In the case of doping with I_2 vapors, only the disappearance of the band present at 774 cm^{-1} was observed, which may imply a partial polarization of those moieties following the same reasoning. Given that the P4VP was not expected to be a rigid skeleton and a non-evident lamellar structure, the charge transfer bands were most likely to arise from relatively local oligomers in which neutral and cation radical TTF moieties came into close contact. Finally, the possibility to reach the P4VP-$TTFCOOH^{0}$-$TTFCOOH^{+\bullet}$ mixed valence intermediated state with different doping agents, allowed us to study the charge transport through the generated gaps after doping process along the pendant TTFs this polymeric composite in the form of thin films (Fig. 9). It is very important to notice that even though studies have been conducted in solution, the feasibility of processing this composite material from the liquid state to a thin solid film is required for further technological applications.

3.3. Film characterization

For consistency in our investigations, an important parameter to be controlled in the preparation of P4VP-TTFCOOH films was the thickness of the samples generated. Indeed, homogeneity and reproducibility of the preparation method were studied in detail employing ellipsometry measurements. Moreover, for Electrostatic Force Microscopy (EFM) experiments a maximum thickness of the film samples was also necessary to avoid artifacts during measurements. The ellipsometry studies were conducted on different samples: neat spin-coated films, the same films after doping with $HAuCl_4$ (aq), and spin-coated pre-oxidized solutions (the latter to create oxidized films with no need for further treatment). The thickness values were 30.6 ± 0.4, 38.2 ± 0.3 and 35.3 ± 0.4 nm, respectively. Variations in the thick-

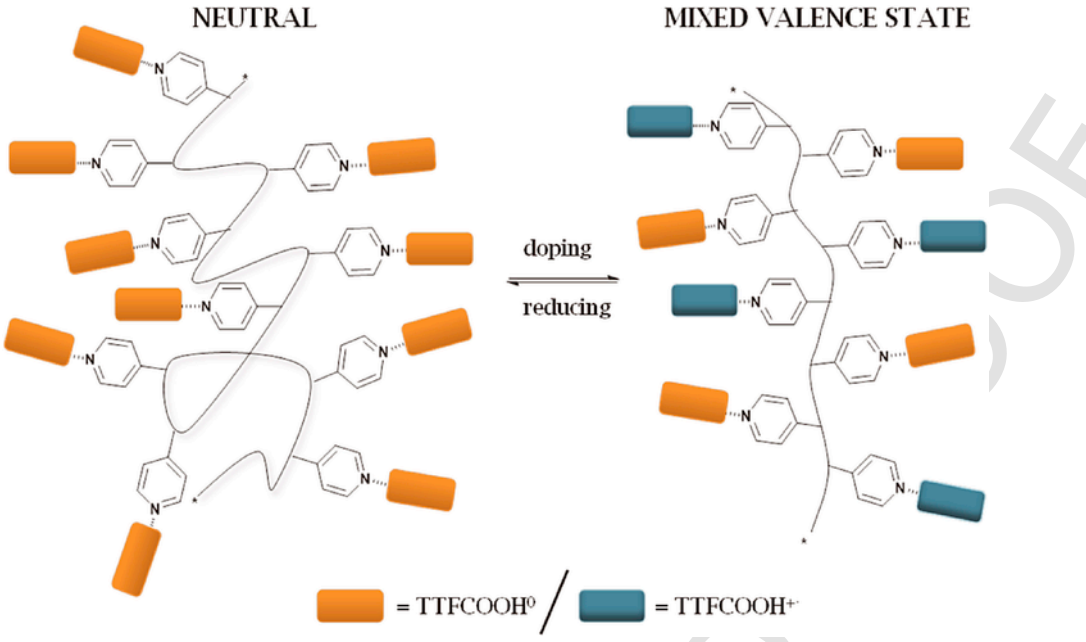

Fig. 9. Representation of P4VP-TTFCOOH^{0}-P4VP-TTFCOOH$^{+\bullet}$ mixed valance state after the doping process.

ness of the undoped and doped films could be a result of different factors such as the incorporation of chloride ions to compensate the charge of TTF cation radicals, the reduction of part of the Au^{3+} to Au^{0} and the incorporation of the metal into the film, as well as, due to a slight swelling of P4VP in aqueous media.

Towards the study of the homogeneity and the structure of P4VP-TTFCOOH films before and after doping, Transmission Electron Microscopy (TEM) measurements were used (see Supp. Info. for details). As shown in Fig. S5, a uniform film was generated before doping. After doping, some branch-shaped structures grew in the film (Fig. S5), attributed to the reduction of Au^{3+} to Au^{0} [44].

In order to confirm the nature of these branch-shaped structures, Scanning Electron Microscopy (SEM) and Energy-dispersive X-ray (EDX) spectroscopy studies were conducted on P4VP-TTFCOOH films doped with $HAuCl_4$ (aq). The corresponding SEM images and EDX analysis revealed a mixed composition of carbon, chlorine, nitrogen, oxygen, sulfur and gold, suggesting the formation of TTF-Au hybrid structures upon oxidation of TTFCOOH and the reduction of Au^{3+} (Fig. S6). Similar results had been previously reported in the literature; however the authors based their studies in solution and on stand-alone pure TTF molecules that resulted in the formation of TTF-Au hybrid wires [45,46]. In the present case, the presence of the polymer conditioned the resulting TTF-Au hybrid structures that self-assembled in a different fashion producing plate-like aggregates.

After the chemical and structural characterization of P4VP-TTFCOOH in solution and solid state, Electrostatic Force Microscopy (EFM) was used to demonstrate that TTF-based polymeric thin films could be used as charge transfer material upon doping (see Supplementary Information for details). The EFM measurements were performed with a single-pass scan in which topographic and electrostatic measurements are obtained at the same time through different order modes [47]. With the aim of understanding the effect of the doping process on P4VP-TTFCOOH films, EFM measurements were performed on undoped P4VP-TTFCOOH films deposited onto graphite (HOPG) by spin-coating (Fig. 10a, Fig. S7) as well as $HAuCl_4$ (Fig. 10b, Fig. S9c), $Fe(ClO_4)_3$ (Fig. 10c, Fig. S11) and I_2 vapors doped P4VP-TTFCOOH films (Fig. 10d, Fig. S12). Firstly, EFM measurements were performed using undoped P4VP-TTFCOOH films (as-spin-coated). The images collected corresponding to the topography (Fig. S7a), amplitude (Fig. 10a, Fig. S7b), phase (Fig. S7c) and the absolute height profiles of the films (Fig. S7d) showed that they were homogeneous.

To discard any signal as a result of the swelling of P4VP during the oxidation process, control experiments were performed using a spin-coated film of P4VP-TTFCOOH on HOPG. The film was then immersed in pure aqueous solution for 10 min, confirming that no changes were appreciated by EFM, hence ensuring that future observations will result directly from the doped P4VP-TTFCOOH hybrid thin films (Fig. S8).

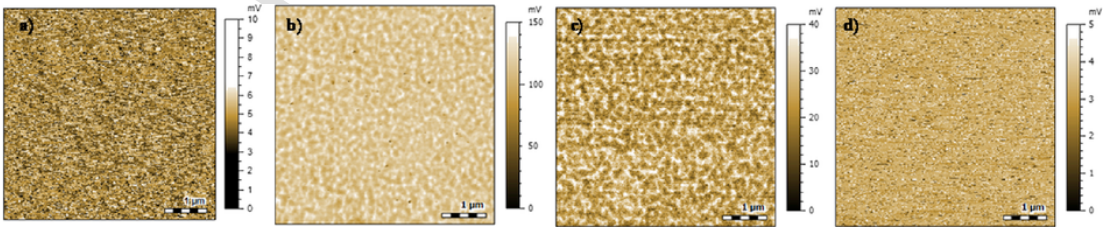

Fig. 10. EFM amplitude images of P4VP-TTFCOOH films: (a) undoped, (b) $HAuCl_4$ (aq) doped, (c) $Fe(ClO_4)_3$ (aq) doped and (d) I_2 doped. The scales of the axis were adjusted to maximise the contrast.

The effect of $HAuCl_4$ doping on P4VP-TTFCOOH films resulted in drastic changes in topography, phase and amplitude as shown with EFM studies (Fig. 10b, Fig. S9). The increase of the roughness that the topography depicted was attributed to both, the tendency of TTF-COOH to self-assemble between their neighboring units and to the non-negligible effect of the water, which did not affect the polymer by itself (according to EFM results depicted in Fig. S8) but it did to TTFCOOH molecules with the formation of charge transfer slats (Fig. S9a-b) [48]. In the amplitude response, the high contrast values indicated the formation of mixed valence states between $TTFCOOH^0$ and $TTFCOOH^{+\bullet}$ units, suggesting that charge transport on these films can be achieved. Under a certain electric field, a tunnel barrier effect was produced as a result of the charge transport between $TTFCOOH^0$ and $TTFCOOH^{+\bullet}$ (Fig. S9c). Later on, this charge was accumulated, and reversibly tunnelled out when an opposite electric field was applied, recovering initial values. To corroborate that the topographic signal was not due to a result of cross-talking with the amplitude response, the amplitude profile was measured and compared with the height profile (Fig. S9d) (the same onset and offset points as the height profile were taken). No correlation between the two profiles could be observed, and therefore, no significant cross-talking was produced. A higher contrast was noticed in the first order phase emphasizing the new organization of the doped films and distinguishing their different nature (Fig. S9e). Moreover, some circular particles attributed to Au^0 particles were found as black spots in the amplitude image of the topography in some areas of the film, indicating a densely charged material (Fig. S9g). In the areas surrounding the particles a dark grey-contrast was observed. One possible explanation for these features was the selective doping in the areas closed to the gold, as inferred in the TEM measurements. The non-equivalent size of these dark areas with respect to the size of the particles in the surrounding material, the P4VP-TTFCOOH, suggested that it might be a response of the doped $TTFCOOH^0$-$TTFCOOH^{+\bullet}$, according to the analysed results.

The EFM technique allowed a complementary study of the relationship between tip bias and the amplitude. Plotting the curves of amplitude-tip bias is helpful to analyse qualitatively the amplitude response of the film to an applied voltage. Comparing the amplitude response curve from HOPG and undoped films (Fig. 11, Fig. S9f), a completely different behaviour of the doped films was evident. The slope of the HOPG curve was ~20 times lower than the corresponding to an undoped film, mainly due to the different conductive response. This effect can be explained as result of the reduced conductivity of the surface due to the presence of a dielectric organic thin film on HOPG. The dark areas from the doped film, corresponding to the areas close to the metallic particles, had a lower slope (~2 times) than the bright areas from the same sample and approximately 10 times lower than the undoped film. Moreover, this slope was at least 2 times higher than that of HOPG. Taking as a reference the HOPG curve, it could be proved that the dark areas of the doped film could behave as charge carriers when sufficient bias was applied to the sample. A shift in the tip bias values (corresponding to the minimum of amplitude) was also evident. Certainly this hysteresis depends, for instance, on the thickness of the film, on the type of bonding to the surface, on the chemical composition, and on the dielectric constant of the tunnel barrier [49]. However, the different shifts observed in the curves of the bright and dark areas presented in Fig. S9c, with respect to the centred position, together with changes in the slope values of the curve for the undoped film, suggested a correlation of the charge carrier character of the film under an electric field [50–52]. In the particular case of curves measured on the bright areas, a deviation of the amplitude at large biases was observed due to a mismatch in the output amplitude channel. Nevertheless, it was the only deviation observed in the samples measured.

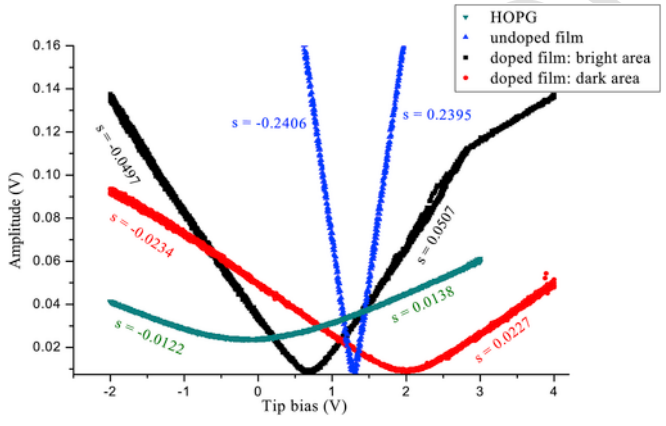

Fig. 11. Amplitude vs. tip bias curves on HOPG, on an undoped film and a $HAuCl_4$ doped film (value following s is the calculated slope). For the same doped sample, values from the brighter and the darker areas were measured.

With the aim to corroborate the tunnel effect produced due to the charge transport in the dark areas of the doped P4VP-TTFCOOH films; several amplitude-tip bias curves (one after the other) were also collected at intervals of 1 s (Fig. S10). Effectively, a shift, an increasing of the slope, and a progressive sharpening of the curves after the third bias sequentially applied could be observed. This observation implied that charge was accumulated on the surface of the film, induced by the bias applied between the tip and the conductive substrate. When a bias was applied sequentially, the charge was continuously accumulated in the areas closest to the tip, until not enough time was given for the tunneling out of this charge or that the inverse voltage applied was not strong enough. After the third curve, no significant additional changes were observed. Comparing the shape and the position of last collected curve with the curves obtained from HOPG and the neat undoped film, we could conclude that the undoped films were clearly much less conductive than HOPG, while $HAuCl_4$ (aq) doped films presented some areas that have charge transportation.

The same EFM studies were performed with films doped with the other oxidants, $Fe(ClO_4)_3$ (Fig. S11) and I_2 vapors (Fig. S12). After doping with $Fe(ClO_4)_3$ (aq), a significant change in the topography (roughness), as well as a dramatic change in the amplitude were observed (Fig. S11a-c). The changes in the topography were related with the self-assembly of the doped pendant TTFCOOH units in order to favor the charge delocalization between $TTFCOOH^0$-$TTFCOOH^{+\bullet}$ pairs. Correlation between the height and amplitude profiles (Fig. S11b-d) could not be observed, similarly to Au^{3+} doped samples (Fig. S9b-d), indicating as well that no cross-talking was obtained. On the other hand, the phase image agreed with the observed changes in roughness and amplitude. Observing the amplitude vs. tip bias curves for the film doped with $Fe(ClO_4)_3$ (Fig. S11f), the same tendency as found for Au^{3+} doped samples was observed but with less differences between the films before and after doping. The amplitude response of undoped films reached its minimum value at 0.105 V, whereas after doping, this value shifted approximately −0.500 V and the hysteresis of the minimum amplitude values between brighter and darker areas was of 0.120 V. These important observations in the hysteresis of the amplitude minimums and slight change of the slope of the curves, which followed the same reasoning process previously discussed for $HAuCl_4$ doped samples, proved that the results obtained were not isolated results and that are not an effect of the influence of

the reduction of Au^{3+} to Au^0. Thus, certainly doped P4VP-TTFCOOH films can lead to materials with charge transport properties through the formation of packed $TTFCOOH^0$-$TTFCOOH^{+\cdot}$ pairs. For $Fe(ClO_4)_3$ doped P4VP-TTFCOOH films, the absence of Fe^{3+} in the EDX spectra, upon doping of film, suggested that Fe^{3+} is reduced to Fe^{2+}, which stayed in the doping solution.

It has been shown that under appropriate conditions P4VP-TTFCOOH films could be doped to mixed valance states $TTFCOOH^0$-$TTFCOOH^{+\bullet}$ when $HAuCl_4$ and $Fe(ClO_4)_3$ were used as oxidants. In contrast, it was not possible to observe a similar effect after doping with I_2 vapors (Fig. S12). The amplitude vs. bias curves before and after doping were only slightly shifted (in the same sense as the other doped films) accompanied by a slight increase in the surface roughness. This suggested that a less effective doping of the film was achieved when the oxidation was conducted with I_2 vapors, indicating that a better arrangement of the polymer and diffusion of the oxidant are necessary for charge transportation.

Finally, Electron Paramagnetic Resonance (EPR) was used as complementary technique to measure the unpaired electrons of doped TTFCOOH moieties in the films. EPR signals of undoped films and films doped with $HAuCl_4$, $Fe(ClO_4)_3$ and I_2 vapors are shown in Fig. 12. The EPR spectrum corresponding to undoped film showed a very low intensity signal that had an average g value of 2.007 (composed of 2.011, 2.008, and 2.003) and a band width (Δ Hpp) of 16 G. A signal and a splitting in the energy intensity of the bands were observed although in principle the compound was neutral. A possible explanation for this phenomenon is that P4VP-TTFCOOH in solution or in film state has suffered a slight oxidation, due to the presence of O_2 (manipulation of the samples was made in air).

On the other hand, $HAuCl_4$, $Fe(ClO_4)_3$ and I_2 doped films had averaged g and Δ Hpp values of 2.007 and 11.9 G, 2.007 and 16 G, and 2.007 and 11.9 G, respectively. As it is shown in the EPR spectra presented in Fig. 12, when the films were oxidized with the different oxidizing agents the intensity of the EPR signals increased dramatically when compared with the as-deposited and undoped P4VP-TTFCOOH films. This increment in the free electron signal was a clear result of the formation of $TTF^{+\bullet}$ species [53].

Comparing all the EPR spectra for the different doping agents used, it was confirmed that $HAuCl_4$ provided a more efficient doping.

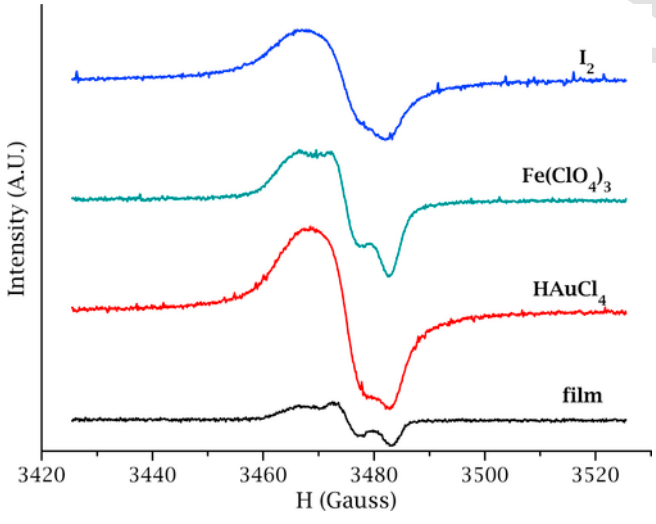

Fig. 12. EPR spectra of P4VP-TTFCOOH film, I_2 doped P4VP-TTFCOOH film, $Fe(ClO_4)_3$ doped P4VP-TTFCOOH film and $HAuCl_4$ doped P4VP-TTFCOOH film on glass slides.

The EPR spectrum of the film oxidized with $HAuCl_4$ presented a greater area of peaks, which is related with the number of the cation-radicals in the sample. The higher presence of cation-radicals favored a more significant concentration of areas with a high magnetic interaction between the species [29,32,40,54,55]. Moreover, the line shape suggested a similar packing between $TTFCOOH$-$TTFCOOH^{+\bullet}$ units regardless of the doping agent used, with the exception of iodine, in line with the results obtained from EFM measurements.

4. Conclusions

It has been demonstrated that the supramolecular functionalization of P4VP polymer with a TTF derivative through complementary hydrogen bonding components is a viable strategy for the preparation of solutions and stable films which incorporate redox active components. Moreover, we show that homogenous and stable thin films with a range of thickness values comprised between 30 and 40 nm can be achieved by spin-coating. Both as films and in solution, TTF moieties could form mixed valence states after doping P4VP-TTFCOOH. In doped P4VP-TTFCOOH films, mixed valence states such as $TTFCOOH^0$-$TTFCOOH^{+\bullet}$ and $TTFCOOH^{+\bullet}$-$TTFCOOH^{2+}$ were confirmed by the appearance of the charge transfer bands in UV-Vis-NIR absorption spectroscopy, however these states could not be observed in P4VP-TTFCOOH doped solutions. This difference between solid state and solution was attributed to a major mobility of the polymeric structure in the latest, which promoted a less controlled and fast doping effect. Contrarily, P4VP-TTFCOOH films reduced the velocity of the oxidation process due to the limited access of the doping agents to all TTFCOOH units, providing a certain control of the different valences of TTFs reached, and thus, permitting the observation of charge transfer bands. UV-Vis-NIR spectroscopy also demonstrated that drop-casted P4VP-TTFCOOH films could be indistinctly doped by sequential cycles of immersion into aqueous salts of Au^{3+}, Fe^{3+} and by exposition to I_2 vapors.

EFM studies of spin-coated P4VP-TTFCOOH thin films indicated that a reorganisation at the surface of the films took place. This phenomenon was correlated to the self-assembly tendency of TTFs in the mixed valence state which facilitates charge motion. Moreover, the electrostatic measurements acquired with the EFM technique also demonstrated that superficial charge inhomogeneities in doped P4VP-TTFCOOH thin films could be associated to a charge-transport phenomenon directly derived from the oxidation process. After analysing the results obtained with UV-Vis-NIR spectra, EPR and EFM results, $HAuCl_4$ and $Fe(ClO_4)_3$ were concluded to be the most effective doping agents to achieve TTFCOOH mixed valence states due to their indistinctly effectiveness in drop-casted and spin-coated films.

Acknowledgments

MRM and AGC thank the CSIC for a JAE Predoc and a JAE-DOC grant, respectively. JPL thanks the MINECO for a Ramon y Cajal contract (RYC-2011-08071). The work was supported by MINECO for project MAT2013-47869-C4-2-P. AGC acknowledges financial support from the Spanish Ministry of Economy and Competitiveness, through the "Severo Ochoa" Programme for Centres of Excellence in R&D (SEV- 2015-0496)"

Appendix A. Supplementary data

Supplementary data related to this article can be found at http://dx.doi.org/10.1016/j.polymer.2016.09.039.

References

[1] J. Frechet, Functional polymers and dendrimers: reactivity, molecular architecture, and interfacial energy, Science 263 (1994) 1710–1715.

[2] J.-T. Chen, C.-S. Hsu, Conjugated polymer nanostructures for organic solar cell applications, Polym. Chem. 2 (2011) 2707–2722.

[3] D.C. Coffey, D.S. Ginger, Time-resolved electrostatic force microscopy of polymer solar cells, Nature Mater. 5 (2006) 735–740.

[4] J. Ruokolainen, G. ten Brinke, O. Ikkala, M. Torkkeli, R. Serimaa, Mesomorphic structures in flexible Polymer−Surfactant systems due to hydrogen Bonding: poly(4-vinylpyridine)−pentadecylphenol, Macromolecules 29 (1996) 3409–3415.

[5] B.J. Rancatore, C.E. Mauldin, S.-H. Tung, C. Wang, A. Hexemer, J. Strzalka, J.M.J. Fréchet, T. Xu, Nanostructured organic semiconductors via directed supramolecular assembly, ACS Nano 4 (2010) 2721–2729.

[6] C.-H. Yu, Y.-H. Chuang, S.-H. Tung, Self-assembly of polystyrene-b-poly(4-vinylpyridine) in deoxycholic acid melt, Polymer 52 (2011) 3994–4000.

[7] H. Sugiyama, H. Kamogawa, Studies on polymers containing functional groups. III. Charge-transfer interaction between quinone and aza polymers, Polym. Sci. A Polym. Chem. 4 (1966) 2281–2288.

[8] J.M.J. Fréchet, M.V. de Meftahi, Poly(vinyl pyridine)s: simple reactive polymers with multiple applications, Brit. Polym. J. 16 (1984) 193–198.

[9] X. Liu, X. Chen, J. Wang, G. Chen, H. Zhang, Hydrogen-bonded polymers with bent-shaped side chains and poly(4-vinylpridine) backbone: phase behavior and thin film morphologies, Macromolecules 47 (2014) 3917–3925.

[10] W. Slough, Charge-transfer complexes of linear polymers, Trans. Faraday Soc. 58 (1962) 2360–2369.

[11] R. Narayan, P. Kumar, K.S. Narayan, S.K. Asha, Supramolecular P4VP-pentadecylphenol naphthalenebisimide comb-polymer: mesoscopic organization and charge transport properties, J. Mater. Chem. C 2 (2014) 6511–6519.

[12] M. Sallé, D. Canevet, J.-Y. Balandier, J. Lyskawa, G. Trippé, S. Goeb, F. Le Derf, Tetrathiafulvalene-based architectures: from guests recognition to self-assembly, Phosphorus Sulfur Silicon Relat. Elem. 186 (2011) 1153–1168.

[13] Y. Mina, M. Yoshiyuki, S. Matthias, Enhanced dipole moments in photo-excited TTF-TCNQ dimers, New J. Phys. 13 (2011) 073039.

[14] H.A.J. Govers, C.G. de Kruif, Intermolecular energy and structure of tetrathiafulvalene (TTF) stacks from atom-atom potentials, Acta Cryst. A 36 (1980) 428–432.

[15] J.B. Torrance, B.A. Scott, B. Welber, F.B. Kaufman, P.E. Seiden, Optical properties of the radical cation tetrathiafulvalenium (TTF+) in its mixed-valence and monovalence halide salts, Phys. Rev. B 19 (1979) 730–741.

[16] S.-L. Cai, Y.-B. Zhang, A.B. Pun, B. He, J. Yang, F.M. Toma, I.D. Sharp, O.M. Yaghi, J. Fan, S.-R. Zheng, W.-G. Zhang, Y. Liu, Tunable electrical conductivity in oriented thin films of tetrathiafulvalene-based covalent organic framework, Chem. Sci. 5 (2014) 4693–4700.

[17] Y. Yokota, K.I. Fukui, T. Enoki, M. Hara, Strong intermolecular electronic coupling within a tetrathiafulvalene Island embedded in self-assembled monolayers, J. Am. Chem. Soc. 129 (2007) 6571–6575.

[18] K. Tanaka, F. Ishiguro, Y. Chujo, Facile preparation of concentration-gradient materials with radical spin of the mixed-valence tetrathiafulvalene in conventional polymer films, Langmuir 26 (2010) 10254–10258.

[19] K. Tanaka, T. Matsumoto, Y. Chujo, Synthesis of highly transparent conductive films with strong absorption in near-infrared region based on tetrathiafulvalene-tethered pendant-type polymers, Synth. Met. 163 (2013) 13–18.

[20] S. Inagi, K. Naka, Y. Chujo, Functional polymers based on electron-donating TTF and derivatives, J. Mater. Chem. 17 (2007) 4122–4135.

[21] K. Tanaka, F. Ishiguro, T. Kunita, Y. Chujo, Transparent conductive films based on polymer composites containing the mixed-valence tetrathiafulvalene nanofibers, J. Polym. Sci. A Polym. Chem. 47 (2009) 6441–6450.

[22] M. Fujihira, Kelvin Probe force microscopy of molecular surfaces, Annu. Rev. Mater. Sci. 29 (1999) 353–380.

[23] S.K. Varshney, X.F. Zhong, A. Eisenberg, Anionic Homopolymerization, Block Copolymerization, Of 4-Vinylpyridine and its investigation by high-temperature size-exclusion chromatography in N-Methyl-2-pyrrolidinone, Macromolecules 26 (1993) 701–706.

[24] T. Kato, J.M.J. Frechet, Stabilization of a liquid-crystalline phase through noncovalent interaction with a polymer side chain, Macromolecules 22 (1989) 3818–3819.

[25] T. Kato, H. Kihara, U. Kumar, T. Uryu, J.M.J. Fréchet, A liquid-crystalline polymer network built by molecular self-assembly through intermolecular hydrogen bonding, Angew. Chem. Int. Ed. 33 (1994) 1644–1645.

[26] S. Malik, P.K. Dhal, R.A. Mashelkar, Hydrogen-bonding-mediated generation of side chain liquid crystalline polymers from complementary nonmesogenic precursors, Macromolecules 28 (1995) 2159–2164.

[27] F.A. Brandys, C.G. Bazuin, Mixtures of an acid-functionalized mesogen with poly(4-vinylpyridine), Chem. Mater. 8 (1996) 83–92.

[28] A. Laforgue, C.G. Bazuin, R.E. Prud'homme, A study of the supramolecular approach in controlling diblock copolymer nanopatterning and nanoporosity on surfaces, Macromolecule 39 (2006) 6473–6482.

[29] R. Bozio, I. Zanon, A. Girlando, C. Pecile, Vibrational spectroscopy of molecular constituents of one-dimensional organic conductors. Tetrathiofulvalene (TTF), TTF+, and (TTF+)2 dimer, J. Chem. Phys. 71 (1979) 2282–2293.

[30] Q.-Y. Zhu, Q.-H. Han, M.-Y. Shao, J. Gu, Z. Shi, J. Dai, Supramolecular and redox chemistry of tetrathiafulvalene monocarboxylic acid with hydrogen-bonded pyridine and bipyridine molecules, J. Phys. Chem. B 116 (2012) 4239–4247.

[31] B. Yameen, M. Ali, R. Neumann, W. Ensinger, W. Knoll, O. Azzaroni, Synthetic proton-gated ion channels via single solid-state nanochannels modified with responsive polymer brushes, Nano Lett. 9 (2009) 2788–2793.

[32] E. Gomar-Nadal, L. Mugica, J. Vidal-Gancedo, J. Casado, N.J.T.L.J. Veciana, C. Rovira, D.B. Amabilino, Synthesis and doping of a multifunctional tetrathiafulvalene- substituted poly(isocyanide), Macromolecules 40 (2007) 7521–7531.

[33] E. Gomar-Nadal, J. Veciana, C. Rovira, D.B. Amabilino, Chiral teleinduction in the formation of a macromolecular multistate chiroptical redox switch, Adv. Mater. 17 (2005) 2095–2098.

[34] J. Puigmarti-Luis, V. Laukhin, A. Perez del Pino, J. Vidal-Gancedo, C. Rovira, E. Laukhina, D.B. Amabilino, Supramolecular conducting nanowires from organogels, Angew. Chem. Int. Ed. 46 (2007) 238–241.

[35] M.S.A. Abdou, S. Holdcroft, Oxidation of π-conjugated polymers with gold trichloride: enhanced stability of the electronically conducting state and electroless deposition of Au^0, Synth. Met. 60 (1993) 93–96.

[36] L.M. Goldenberg, V.Y. Khodorkovsky, J.Y. Becker, M.R. Bryce, M.C. Petty, Semi-conducting Langmuir–Blodgett films of a novel amphiphilic bis(tetrathiafulvalene) derivative, J. Mater. Chem. 5 (1995) 191–192.

[37] R.S. Mulliken, Molecular compounds and their spectra. III. The interaction of electron donors and acceptors, J. Phys. Chem. 56 (1952) 801–822.

[38] V. Khodorkovsky, L. Shapiro, P. Krief, A. Shames, G. Mabon, A. Gorgues, M. Giffard, Do π-dimers of tetrathiafulvalene cation radicals really exist at room temperature, Chem. Commun. (2001) 2736–2737.

[39] T. Kitamura, S. Nakaso, N. Mizoshita, Y. Tochigi, T. Shimomura, M. Moriyama, K. Ito, T. Kato, Electroactive supramolecular self-assembled fibers comprised of doped tetrathiafulvalene-based gelators, J. Am. Chem. Soc. 127 (2005) 14769–14775.

[40] C.-K. Jeong, Y.-I. Kim, Synthesis and characterization of bis(ethylenedithio)tetrathiafulvalene charge transfer compounds with gold, platinum and osmium chloride, Bull. Korean Chem. Soc. 20 (1999) 1509–1512.

[41] M.B. Inoue, M. Inoue, Q. Fernando, K.W. Nebesny, Highly electroconductive tetrathiafulvalenium salts of copper halides, Inorg. Chem. 25 (1986) 3976–3980.

[42] G. Cooke, A.S. Dhindsa, Y.P. Song, G. Williams, A.S. Batsanov, M.R. Bryce, J.A.K. Howard, M.C. Petty, J. Yarwood, Conducting langmuir-blodgett films of new amphiphilic tetrathiafulvalene derivatives, Synth. Met. 57 (1993) 3871–3878.

[43] R.S. Mulliken, Molecular compounds and their spectra. II, J. Am. Chem. Soc. 74 (1952) 811–824.

[44] X. Wang, K. Naka, H. Itoh, S. Park, Y. Chujo, Synthesis of silver dendritic nanostructures protected by tetrathiafulvalene, Chem. Commun. (2002) 1300–1301.

[45] K. Naka, D. Ando, X. Wang, Y. Chujo, Synthesis of organic-metal hybrid nanowires by cooperative self-organization of tetrathiafulvalene and metallic gold via charge-transfer, Langmuir 23 (2007) 3450–3454.

[46] J. Puigmartí-Luis, D. Schaffhauser, B.R. Burg, P.S. Dittrich, A microfluidic approach for the formation of conductive nanowires and hollow hybrid structures, Adv. Mater. 22 (2010) 2255–2259.

[47] M.J. Cadena, R. Misiego, K.C. Smith, A. Avila, B. Pipes, R. Reifenberger, A. Raman, Sub-surface imaging of carbon nanotube–polymer composites using dynamic AFM methods, Nanotechnology 24 (2013) 135706.

[48] M.M.S. Abdel-Mottaleb, E. Gomar-Nadal, M. Surin, H. Ujii, W. Mamdouh, J. Veciana, V. Lemaur, C. Rovira, J. Cornil, R. Lazzaroni, D.B. Amabilino, S. De Feyter, F.C. De Schryver, Self-assembly of tetrathiafulvalene derivatives at a liquid/solid interface—compositional and constitutional influence on supramolecular ordering, J. Mater. Chem. 15 (2005) 4601–4615.

[49] A. Roy-Gobeil, Y. Miyahara, P. Grutter, Revealing energy level structure of individual quantum dots by tunneling rate measured by single-electron sensitive electrostatic force spectroscopy, Nano Lett. 15 (2015) 2324–2328.

[50] R. Dianoux, F. Martins, F. Marchi, C. Alandi, F. Comin, J. Chevrier, Detection of electrostatic forces with an atomic force microscope: analytical and experimental dynamic force curves in the nonlinear regime, Phys. Rev. B 68 (2003) 045403.

[51] I.H. Campbell, J.D. Kress, R.L. Martin, D.L. Smith, N.N. Barashkov, J.P. Ferraris, Controlling charge injection in organic electronic devices using self-assembled monolayers, Appl. Phys. Lett. 71 (1997) 3528.

[52] L. Collins, M.B. Okatan, Q. Li, Q. Kravenchenko II, N.V. Lavrik, S.V. Kalinin, B.J. Rodriguez, S. Jesse, Quantitative 3D-KPFM imaging with simultaneous electrostatic force and force gradient detection, Nanotechnology 26 (2015) 175707.

[53] L. Ćavara, F. Gerson, D.O. Cowan, K. Lerstrup, An ESR study of the radical cations of tetrathiafulvalene (TTF) and electron donors containing the TTF moiety, Helv. Chim. Acta 69 (1986) 141–151.
[54] Y. Harima, Y. Kunugi, H. Tang, K. Yamashita, M. Shiotani, J. Ohshita, A. Kunai, Transport and in situ ESR studies on polymer film composed of quinquethiophenes bridged by monosilanylene units, Synth. Met. 113 (2000) 173–183.
[55] C. Rovira, J. Veciana, N. Santalo, J. Tarres, J. Cirujeda, E. Molins, J. Llorca, E. Espinosa, Synthesis of several isomeric tetrathiafulvalene.pi.-electron donors with peripheral sulfur atoms. A study of their radical cations, J. Org. Chem. 59 (1994) 3307–3313.